

# CLIPoint3D: Language-Grounded Few-Shot Unsupervised 3D Point Cloud Domain Adaptation

\*Mainak Singha<sup>1</sup>\*Sarthak Mehrotra<sup>2</sup>Paolo Casari<sup>1,3</sup>Subhasis Chaudhuri<sup>4</sup>Elisa Ricci<sup>1,5</sup>Biplab Banerjee<sup>4</sup><sup>1</sup> University of Trento, Italy <sup>2</sup> MDSR Labs Adobe, India <sup>3</sup> CNIT, Italy <sup>4</sup> IIT Bombay, India <sup>5</sup> Fondazione Bruno Kessler, Italy

## Abstract

Recent vision-language models (VLMs) such as CLIP demonstrate impressive cross-modal reasoning, extending beyond images to 3D perception. Yet, these models remain fragile under domain shifts, especially when adapting from synthetic to real-world point clouds. Conventional 3D domain adaptation approaches rely on heavy trainable encoders, yielding strong accuracy but at the cost of efficiency. We introduce **CLIPoint3D**, the first framework for few-shot unsupervised 3D point cloud domain adaptation built upon CLIP. Our approach projects 3D samples into multiple depth maps and exploits the frozen CLIP backbone, refined through a knowledge-driven prompt tuning scheme that integrates high-level language priors with geometric cues from a lightweight 3D encoder. To adapt task-specific features effectively, we apply parameter-efficient fine-tuning to CLIP’s encoders and design an entropy-guided view sampling strategy for selecting confident projections. Furthermore, an optimal transport-based alignment loss collaboratively bridge source-target distribution gaps while maintaining class separability. Extensive experiments on **PointDA-10** and **GraspNetPC-10** benchmarks show that CLIPoint3D achieves consistent 3-16% accuracy gains over both CLIP-based and conventional encoder-based baselines. Codes are available at <https://github.com/SarthakM320/CLIPoint3D>.

## 1. Introduction

Point cloud understanding underpins modern 3D vision, driving applications in autonomous driving [60], terrain mapping [61], augmented reality, and robotics [59]. Unlike 2D imagery, point clouds explicitly encode fine-grained geometric cues essential for spatial reasoning. Despite the remarkable progress of deep 3D architectures [19, 44, 62], most assume identical training and deployment distribu-

\*equal contribution

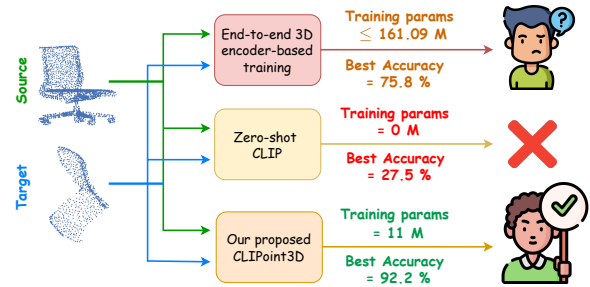


Figure 1. **Comparison of CLIPoint3D with SOTA methods on GraspNetPC-10.** Encoder-based 3D UDA methods (e.g., PointDAN [45], GAST [75], MLSP [36]) are accurate but computationally expensive, while CLIP-based extensions fail to bridge the synthetic-real gap. CLIPoint3D achieves +16.4% improvement with minimal overhead.

tions. In practice, scans acquired from heterogeneous sensors exhibit large variations in point density, sampling patterns, occlusion, and background clutter, leading to severe performance degradation under domain shifts [5, 43]. This issue is exacerbated when transferring from synthetic benchmarks to real-world environments, making *unsupervised domain adaptation (UDA)* [13, 14, 32, 37, 38, 58] central to achieving scalable 3D perception.

Direct fine-tuning on target data can partially mitigate domain gaps but requires dense 3D annotations and high compute, impractical for dynamic or safety-critical applications [3, 48]. Since 3D labeling is costly and error-prone [29], UDA methods aim to transfer knowledge from labeled sources to unlabeled targets. The key difficulty lies in jointly enforcing *statistical alignment* (distributional consistency) and *semantic alignment* (class-level coherence); neglecting either leads to geometrically aligned yet semantically inconsistent features.

However, existing unsupervised point cloud domain adaptation (UPDA) techniques generally fall into three paradigms. (i) *Adversarial alignment* [14, 45] uses domain discriminators to match latent features but often suf-

fers from model collapse and over-alignment. (ii) *Self-supervised learning* [2, 51, 70] employs pretext tasks such as rotation or deformation prediction, but lacks semantic awareness. (iii) *Pseudo-labeling and self-paced learning* [36, 53, 75] iteratively refine noisy labels, yet degrade under large shifts. Although effective in controlled setups, these models are geometry-centric, computationally heavy, and rarely leverage semantic priors or uncertainty estimation, limiting their robustness to unseen modalities.

Recently, vision-language models (VLMs) such as CLIP [47] have demonstrated impressive zero-shot transfer by coupling visual and textual modalities through large-scale contrastive pretraining. Extending CLIP to 3D [22, 25, 52, 71, 74] typically involves projecting point clouds into multi-view depth maps and processing them via CLIP’s image encoder. While effective for single-domain tasks, such projections expose two fundamental limitations: (i) **Modality gap**: CLIP’s encoder, trained on RGB images, poorly captures the sparse, textureless, and geometry-dominant nature of 3D depth maps; (ii) **Domain gap**: Existing CLIP-3D models [7, 64, 65] lack mechanisms for cross-domain adaptation, yielding poor generalization beyond their source domain. These issues reveal a crucial research gap: *How can we harness CLIP’s semantic priors to enable unsupervised 3D domain adaptation while bridging both the 2D-3D modality and source-target domain gaps in a compute-efficient way?*

We hypothesize that CLIP’s language-grounded latent space can be effectively adapted for 3D UDA if jointly guided by geometric cues and uncertainty-aware optimization. This motivates a framework that (i) injects geometric awareness into CLIP’s latent space, (ii) aligns distributions across domains without labels, and (iii) achieves parameter-efficient adaptation for few-shot supervision.

**Our Approach.** We introduce **CLIPoint3D**, a unified framework for *few-shot unsupervised 3D domain adaptation* built on top of CLIP. It projects each point cloud into multiple depth maps [71] and reuses CLIP’s frozen visual backbone, leveraging 2D pretraining for efficient 3D transfer. A *knowledge-driven prompt tuning* module fuses high-level semantic priors from large language models (LLMs) [1, 18, 42, 46, 66] with low-level geometric features from a lightweight 3D encoder, grounding CLIP’s embeddings in 3D structure. To further reduce compute, we employ *parameter-efficient fine-tuning (PEFT)* [35] to adapt a small subset of CLIP parameters while preserving its zero-shot capability. An *entropy-guided view sampling* strategy [54] filters ambiguous or redundant views to stabilize multi-view aggregation. Finally, we introduce two *novel* alignment objectives: (i) an **uncertainty-aware prototype alignment loss** that performs class-level coupling using entropy-weighted prototypes, and (ii) an **entropy-regularized OT alignment** that enforces smooth, noise-

tolerant global matching. Together, these confidence-aware objectives yield robust semantic and distributional alignment under large 3D domain shifts.

In summary, our key contributions are:

1. The first CLIP-based framework for few-shot unsupervised 3D point cloud domain adaptation, achieving strong cross-domain generalization with minimal training cost.
2. A knowledge-driven prompt tuning scheme that unites LLM-derived semantic priors and 3D geometry for multimodal grounding.
3. Dual uncertainty-aware objectives, OT-based statistical alignment and prototype-level semantic regularization, that tighten the adaptation generalization bound (Sec. 3.3).
4. An entropy-guided view selection mechanism that enhances stability, interpretability, and efficiency under multi-view uncertainty.

Extensive experiments and ablations across standard benchmarks demonstrate that CLIPoint3D achieves superior accuracy-efficiency trade-offs compared to both 3D encoder-based and CLIP-based baselines (Figure 1).

## 2. Related Works

### Unsupervised 3D Point Cloud Domain Adaptation.

UPDA seeks to transfer knowledge from labeled source to unlabeled target domains. Existing approaches mainly follow three paradigms. (i) *Domain adversarial training* [14, 45] employs discriminators to enforce feature invariance while the feature extractor learns to confuse them. Although conceptually sound, such methods often suffer from unstable convergence, mode collapse, and over-alignment that compromises geometric fidelity critical for fine-grained 3D recognition. (ii) *Self-supervised learning (SSL)* [2, 51, 70] leverages auxiliary pretext tasks such as rotation prediction [75] or deformation reconstruction [2] to capture domain-invariant cues. While interpretable, SSL mainly learns low-level geometric invariances with limited semantic alignment. (iii) *Pseudo-label and self-paced learning* [36, 53, 75] iteratively refines pseudo labels for confident target samples, but noisy labels under large shifts amplify confirmation bias. Overall, most UPDA methods are geometry-centric, computationally heavy, and lack semantic grounding or uncertainty modeling, making them less effective for lightweight few-shot adaptation.

**CLIP for 3D Understanding.** Large-scale vision-language models such as CLIP [47] learn rich multimodal embeddings by aligning image and text representations, inspiring a range of 3D extensions. PointCLIP [71], PointCLIP v2 [74], DiffCLIP [52], and MVFPoint [9] project 3D point clouds into multi-view depth maps and process them via CLIP’s image encoder, achieving strong zero-/few-shot



2D VLMs like CLIP, pretrained on textured RGB data, to sparse, textureless 3D projections.

### 3.1. Our CLIPoint3D Framework

CLIPoint3D builds upon a frozen CLIP backbone composed of a vision encoder  $\mathcal{E}_v$  and a text encoder  $\mathcal{E}_t$ . Following [71], we employ online perspective projection [17] without any post-rendering operations [57], directly projecting each 3D point onto a set of predefined image planes to produce scatter-based depth maps. For each projected view  $x_{i,m}$  of a 3D point cloud  $\mathbf{PC}_i$ , the vision encoder produces an embedding  $\mathbf{v}_{i,m} = \mathcal{E}_v(x_{i,m}) \in \mathbb{R}^{1 \times d}$ , where  $d$  is the feature dimension. For  $K$  categories, text templates are encoded as  $\mathbf{T} = \mathcal{E}_t(\mathbf{t}) \in \mathbb{R}^{K \times d}$ , with  $\mathbf{t}$  denoting the set of class templates. Given temperature  $\tau$ , the probability of assigning class  $y$  to view  $x_{i,m}$  is:

$$p(y|x_{i,m}) = \frac{\exp(\cos(\mathbf{v}_{i,m}, \mathbf{T}_y)/\tau)}{\sum_{k=1}^K \exp(\cos(\mathbf{v}_{i,m}, \mathbf{T}_k)/\tau)}. \quad (1)$$

To effectively adapt CLIP to 3D understanding under domain shift, CLIPoint3D refines its latent space through four complementary modules (in Figure 2): (i) *Knowledge-driven prompt tuning*, integrating LLM-guided language priors with geometric cues for coherent adaptation of both encoders; (ii) *PEFT*, selectively updating a minimal set of CLIP’s parameters to specialize on multi-view 3D structure; (iii) *Entropy-guided view selection*, filtering uncertain projections to enhance feature consistency; and (iv) *Uncertainty-aware prototype alignment*, aligning source-target domains while preserving class separability.

#### 3.1.1. Knowledge-Driven Prompt Tuning

Conventional prompt-tuning methods [31, 34, 72] adapt pretrained models by inserting lightweight learnable tokens while keeping the backbone frozen. Techniques such as CoOp [73], VPT [26], and MaPLe [27] work well for 2D images because texture strongly correlates with semantics. However, when transferred to sparse 3D projections, these assumptions fail: (i) textual prompts remain purely linguistic without geometric grounding, and (ii) visual prompts depend on texture cues that are absent in point clouds. Consequently, CLIP’s latent space remains biased toward its 2D pretraining distribution and struggles to represent 3D data.

To address this limitation, we propose a *knowledge-driven multimodal prompt-tuning* strategy that links linguistic semantics with 3D structure. We jointly adapt CLIP’s text and vision encoders using two complementary knowledge sources: (a) high-level semantic priors from an LLM [42], and (b) low-level geometric descriptors from a lightweight 3D encoder  $\mathcal{E}_{3D}$  [44]. A shared query vector  $\mathbf{q}$  drives cross-modal attention, ensuring that both textual and visual prompts evolve around a common semantic reference while retaining modality-specific flexibility. This

yields geometry-aware semantic reasoning and stable domain transfer.

→ **Textual Prompt Generation.** For each class label  $y_k \in \mathcal{Y}$ , the LLM generates a descriptive sentence ‘‘a 3D point cloud object of a [CLS] with [attributes]’’, anchoring the prompt explicitly within the 3D modality. The frozen CLIP text encoder  $\mathcal{E}_t^{fz}$  (where  $fz$  denotes frozen) encodes these phrases as:

$$\mathbf{T}^{\text{llm}} = \{\mathcal{E}_t^{fz}(\text{prefix} + \text{LLM}(y_k))\}_{k=1}^K. \quad (2)$$

A text-side multi-head cross-attention (MHCA) module then refines these embeddings using the shared query  $\mathbf{q}$ :

$$\mathbf{P}_t = \text{FFN}(\text{MHCA}(\mathbf{Q}_q, \mathbf{K}_{\mathbf{T}^{\text{llm}}}, \mathbf{V}_{\mathbf{T}^{\text{llm}}}), \quad (3)$$

where  $\mathbf{Q}_q = \mathbf{q}W_{\mathbf{Q}}$ ,  $\mathbf{K}_{\mathbf{T}^{\text{llm}}} = \mathbf{T}^{\text{llm}}W_{\mathbf{K}_t}$ , and  $\mathbf{V}_{\mathbf{T}^{\text{llm}}} = \mathbf{T}^{\text{llm}}W_{\mathbf{V}_t}$ . Here, FFN denotes a feed-forward network. The learned textual prompt  $\mathbf{P}_t$  conditions the text encoder  $\mathcal{E}_t$ , producing geometry-aware, domain-stable embeddings  $\mathbf{T} = \mathcal{E}_t(\mathbf{t}, \mathbf{P}_t)$ .

→ **Visual Prompt Generation.** Given a 3D point cloud  $\mathbf{PC}$ , its structural feature representation  $\mathbf{I}_{3D} = \mathcal{E}_{3D}(\mathbf{PC})$  is injected into a parallel vision-side MHCA block using the same shared query  $\mathbf{q}$ :

$$\mathbf{P}_v = T_{\text{proj}}(\text{FFN}(\text{MHCA}(\mathbf{Q}_q, \mathbf{K}_{\mathbf{I}_{3D}}, \mathbf{V}_{\mathbf{I}_{3D}}))), \quad (4)$$

where  $\mathbf{K}_{\mathbf{I}_{3D}} = \mathbf{I}_{3D}W_{\mathbf{K}_v}$  and  $\mathbf{V}_{\mathbf{I}_{3D}} = \mathbf{I}_{3D}W_{\mathbf{V}_v}$ . The projection layer  $T_{\text{proj}}$  maps  $\mathbf{P}_v$  to CLIP’s patch-embedding dimension, producing geometry-aware visual prompts  $\mathbf{P}_v^S$  and  $\mathbf{P}_v^T$  for source and target domains, respectively. Distinct parameter sets ( $W_{\mathbf{K}_t}, W_{\mathbf{V}_t}$ ) and ( $W_{\mathbf{K}_v}, W_{\mathbf{V}_v}$ ) ensure modality-specific adaptability, while the shared query vector  $\mathbf{q}$  maintains a unified alignment objective.

By fusing LLM-driven semantic hierarchies with invariant 3D structural priors under a shared attention query, CLIPoint3D transforms visual prompt tuning from shallow token reweighting into structured multimodal knowledge transfer. The visual embedding for a projected view of a specific domain becomes  $\mathbf{v}_{i,m} = \mathcal{E}_v(x_{i,m}, \mathbf{P}_v)$ . This yields three notable benefits: (i) enhanced text–vision correspondence under missing appearance cues, (ii) stable cross-domain adaptation through geometry-grounded semantics, and (iii) parameter-efficient adaptation with minimal computational overhead (see Table 5).

#### 3.1.2. Few-Shot PEFT Adaptation

While knowledge-driven prompt tuning aligns linguistic and geometric cues, CLIP’s encoders, pretrained on RGB images and short captions, still struggle to model fine-grained 3D structure. Fully fine-tuning  $\mathcal{E}_v$  on sparse projections risks overfitting and disrupting the pretrained image-text alignment crucial for generalization. To enable targeted geometric adaptation without harming semantic consistency, CLIPoint3D employs a LoRA-based PEFT [24].

$\mathcal{E}_v$  is decomposed into a frozen backbone and lightweight low-rank adapters that capture 3D-specific residual cues such as curvature, surface continuity, and depth transitions. Updating only these adapters stabilizes gradients, reduces parameter cost, and avoids drifting from CLIP’s semantic priors while still modeling domain-dependent geometric variations. We also apply PEFT to  $\mathcal{E}_t$ , whose pretrained space is biased toward 2D natural-image semantics. Low-rank adapters introduce controlled shifts that align LLM-enhanced prompts with 3D structural attributes without perturbing global CLIP alignment. Table 3 shows complementary gains from adapting each branch individually and jointly.

Thus, PEFT serves as the *local adaptation layer* of CLIPoint3D: prompt tuning provides global semantic alignment, while PEFT refines encoder features for domain- and task-specific structure, ensuring the model remains both semantically coherent and geometrically discriminative under few-shot supervision.

### 3.1.3. Entropy-Guided View Selection

In parallel to multimodal prompt tuning and PEFT adaptation, each point cloud  $\mathbf{PC}_i$  is projected into  $M$  depth maps  $\{x_{i,m}\}_{m=1}^M$  for CLIP-based inference. However, not all projections contribute equally occluded or sparsely sampled views often yield ambiguous predictions that distort feature aggregation. To ensure that only structurally reliable projections influence adaptation, CLIPoint3D employs an *entropy-guided view selection* mechanism that filters views based on prediction uncertainty.

For each view  $x_{i,m}$ , the posterior probability  $p(y_k | x_{i,m})$  from Eq. (1) is used to compute predictive entropy:

$$H_{i,m} = - \sum_{k=1}^K p(y_k | x_{i,m}) \log p(y_k | x_{i,m}), \quad (5)$$

where low  $H_{i,m}$  denotes high model confidence and geometric reliability. Views satisfying  $H_{i,m} \leq \tau_\rho$ , where  $\tau_\rho$  is the  $\rho$ -th percentile of entropy values across all  $M$  views of  $\mathbf{PC}_i$  (we use  $\rho = 0.5$ ), form the confident subset  $\mathcal{M}_i^* = \{m | H_{i,m} \leq \tau_\rho\}$ . The class probability for the full point cloud is then aggregated over this selected subset:

$$p(y | \mathbf{PC}_i) = \frac{1}{|\mathcal{M}_i^*|} \sum_{m \in \mathcal{M}_i^*} p(y | x_{i,m}). \quad (6)$$

We use  $p_S$  and  $p_T$  while considering the source and target samples, respectively. This filtering strategy provides a self-adaptive reliability prior, retaining diverse yet confident projections while suppressing noisy or redundant ones. Unlike uniform pooling [71], it introduces no additional parameters and naturally adjusts to domain-dependent uncertainty (see Table 6). Used in both training and inference,

it complements PEFT by supplying uncertainty-aware evidence selection, yielding stable multi-view fusion and generalization.

### 3.1.4. Domain Alignment Strategies

The final stage of CLIPoint3D aligns source and target distributions in CLIP’s multimodal space while explicitly accounting for prediction uncertainty. Prior modules improve view reliability and semantic grounding, yet residual misalignment persists, mainly because conventional adversarial [14] or MMD-based [37] methods treat all samples equally, allowing low-confidence target embeddings to dominate optimization. To address this, we propose an *Uncertainty-Aware Optimal Transport (UA-OT)* framework that introduces two complementary novelties: (i) **entropy-weighted class prototypes** that perform sample-wise confidence filtering at the class level, and (ii) **entropy-regularized OT** that enforces global distribution matching while suppressing noisy couplings. Together, these mechanisms deliver confidence-calibrated alignment unavailable in prior 3D/2D DA methods.

**Entropy-weighted prototype alignment.** Let  $\mathbf{v}_i^S$  and  $\mathbf{v}_j^T$  denote the confident-view aggregated embeddings of source and target clouds (Sec. 3.1.3). Each source cloud is assigned an entropy-based reliability weight,

$$w_i^S = 1 - \frac{H(p_S(y | \mathbf{PC}_i^S))}{\log K}, \quad (7)$$

allowing uncertain samples to be automatically down-weighted. The resulting class-specific prototype is

$$\mathbf{U}_c = \frac{\sum_{i: y_i^S=c} w_i^S \mathbf{v}_i^S}{\sum_{i: y_i^S=c} w_i^S}. \quad (8)$$

Target clouds receive analogous weights and pseudo-labels:

$$w_j^T = 1 - \frac{H(p_T(y | \mathbf{PC}_j^T))}{\log K}, \quad (9)$$

$$\hat{y}_j = \arg \max_c p_T(y = c | \mathbf{PC}_j^T).$$

Prototype alignment is enforced via

$$\mathbf{L}_{\text{proto}} = - \sum_j w_j^T \log \frac{\exp(\cos(\mathbf{v}_j^T, \mathbf{U}_{\hat{y}_j})/\tau)}{\sum_{c'} \exp(\cos(\mathbf{v}_j^T, \mathbf{U}_{c'})/\tau)}. \quad (10)$$

This *uncertainty-weighted class coupling* is a key novelty: high-confidence target clouds drive semantic alignment, while unreliable ones contribute minimally.

**Entropy-regularized optimal transport.** While prototype alignment promotes class-conditional consistency, global distribution mismatch can persist. We therefore apply a second novelty, **entropy-regularized OT over cloud-level**

**embeddings**, which provides smooth, noise-tolerant domain matching. Let

$$C_{ij} = \|\mathbf{v}_i^S - \mathbf{v}_j^T\|_2^2$$

be the transport cost and  $\pi \in \Pi(\mathcal{P}_S, \mathcal{P}_T)$  a feasible plan. The UA-OT loss is

$$\mathbf{L}_{\text{OT}} = \min_{\pi} \left( \langle C, \pi \rangle - \varepsilon H(\pi) \right), \quad (11)$$

where the entropy term  $H(\pi)$  avoids overly sharp couplings and stabilizes the alignment under prediction noise.

**Auxiliary calibration loss.** To further support stable prototype and OT coupling, we minimize the prediction entropy of both domains:

$$\mathbf{L}_{\text{conf}} = \sum_i \mathbb{H}\left(p_S(y | \mathbf{PC}_i^S)\right) + \frac{1}{N_T} \sum_j \mathbb{H}\left(p_T(y | \mathbf{PC}_j^T)\right) \quad (12)$$

The first term yields cleaner source prototypes, while the second encourages compact target clusters that reinforce Eq. 10. Together, entropy-weighted prototypes, entropy-regularized OT, and unified calibration form a robust, confidence-driven alignment mechanism.

### 3.2. Overall Training and Inference

The full optimization objective of CLIPoint3D integrates supervised learning, geometric regularization, and uncertainty-aware alignment in a unified framework. The total loss is

$$\mathbf{L}_{\text{total}} = \mathbf{L}_{\text{ce}} + \alpha(\mathbf{L}_{\text{ortho}} + \mathbf{L}_{\text{proto}} + \mathbf{L}_{\text{OT}} + \mathbf{L}_{\text{conf}}), \quad (13)$$

where  $\mathbf{L}_{\text{ce}}$  is the supervised cross-entropy on source data  $\mathcal{D}_S$ . The geometric consistency term  $\mathbf{L}_{\text{ortho}}$  [44] regularizes the 3D encoder  $\mathcal{E}_{3D}$  by enforcing local feature decorrelation, for both the domains:

$$\mathbf{L}_{\text{ortho}} = \|\mathbf{I}_{3D}^T \mathbf{I}_{3D} - \mathbb{I}\|_2^2, \quad (14)$$

where  $\mathbb{I}$  is the identity matrix.

**Inference.** At test time, each target cloud  $\mathbf{PC}_j^T$  is projected into multiple views, and predictions are aggregated using the entropy-guided selection rule (Eq. 6), yielding a robust multi-view decision.

### 3.3. Generalization Bound

Following classical DA theory [4, 49], for any hypothesis  $h \in \mathcal{H}$  with bounded loss  $\ell \in [0, 1]$ , the source risk is

$$\mathcal{R}_S(h) = \mathbb{E}_{(\mathbf{x}, y) \sim \mathcal{P}_S} [\ell(h(\mathbf{x}), y)]. \quad (15)$$

The corresponding target risk is upper-bounded by

$$\mathcal{R}_T(h) \leq \mathcal{R}_S(h) + \frac{1}{2} d_{\mathcal{H}\Delta\mathcal{H}}(\mathcal{P}_S, \mathcal{P}_T) + \lambda^*, \quad (16)$$

where  $d_{\mathcal{H}\Delta\mathcal{H}}$  measures distributional discrepancy and  $\lambda^*$  is the joint optimal risk over  $\mathcal{H}$ .

In CLIPoint3D, the entropy-regularized OT loss  $W_{\varepsilon}(\mathcal{P}_S, \mathcal{P}_T)$  serves as a smooth surrogate for  $d_{\mathcal{H}\Delta\mathcal{H}}$ , providing a stable measure of global domain shift. Complementarily, the uncertainty-weighted prototype alignment suppresses noisy features and encourages class-conditional consistency, thereby reducing the discrepancy contributing to  $\lambda^*$ . Let  $\mathbf{U}_c^S$  and  $\mathbf{U}_c^T$  denote entropy-weighted source and pseudo-labeled target prototypes; their agreement enforces tight semantic coupling across domains.

Under these relaxations, the resulting surrogate bound becomes

$$\mathcal{R}_T(h) \leq \mathcal{R}_S(h) + \frac{1}{2} W_{\varepsilon}(\mathcal{P}_S, \mathcal{P}_T) + \beta \sum_{c=1}^K \|\mathbf{U}_c^S - \mathbf{U}_c^T\|_2^2, \quad (17)$$

where  $\beta$  trades off global (OT) and semantic (prototype) alignment. Entropy-guided view selection lowers  $\mathcal{R}_S(h)$  by filtering uncertain projections. Together, these components yield a tighter, uncertainty-aware bound and support reliable transfer of CLIP’s 2D priors into the 3D setting. See Supplementary for further discussions.

## 4. Experimental Evaluation

**Datasets:** We evaluate our proposed method on two domain adaptation benchmarks: PointDA-10 [45] and GraspNetPC-10 [53]. The PointDA-10 benchmark consists of three widely used PC datasets: ModelNet [63], ShapeNet [6], and ScanNet [8]. In contrast, GraspNetPC-10, derived from GraspNet [11] by [53], includes three distinct domains: Synthetic, Kinect, and RealSense. Both benchmarks share the same 10 object categories across all domains. Further details are provided in the Supplementary.

**Implementation Details and Evaluation Metric:** In our experiments, we employ the frozen ViT-B/16 variant of the CLIP backbone, PointNet [44] as the 3D encoder, and GPT-5 [42] as the LLM. Each multi-head cross-attention block comprises four attention heads, followed by layer normalization and an FFN with a two-layer bottleneck structure (Linear-GeLU-Linear). We use  $M = 10$  projected depth maps for each point cloud sample. The learnable query vector  $\mathbf{q}$  has a length of 4 and dimensionality of 512. For parameter-efficient fine-tuning, we adopt LoRA [24] with a rank of 16 and dropout rate of 0.1. In Eq. 13, the loss balancing coefficient is set to  $\alpha = 1$ . Training is performed with a batch size of 32, 64 shots per class, and for a total of 50 epochs. The learning rate is initialized at 0.002 with a decay rate of  $1 \times 10^{-5}$ , momentum of 0.9, and the SGD [50] optimizer. We report the classification performance in the target domain as the evaluation metric. Reported results are averaged over three runs.

Table 1. **Domain adaptation performance on the PointDA-10 benchmark.** M: ModelNet, S: ShapeNet, S\*: ScanNet;  $\rightarrow$  indicates the adaptation direction. Best results and second-best results are reported in bold and underlined, respectively.

Methods	M $\rightarrow$ S	M $\rightarrow$ S*	S $\rightarrow$ M	S $\rightarrow$ S*	S* $\rightarrow$ M	S* $\rightarrow$ S	Avg
DANN [14]	74.8	42.1	57.5	50.9	43.7	71.6	56.8
PointDAN [45]	83.9	44.8	63.3	45.7	43.6	56.4	56.3
RS [51]	79.9	46.7	75.2	51.4	71.8	71.2	66.0
DAE-Global [20]	83.5	42.6	74.8	45.5	64.9	67.3	63.1
DefRec [2]	82.7	43.9	<u>79.8</u>	48.0	66.0	67.4	64.6
DefRec + PCM [2]	83.3	53.5	78.5	53.2	73.7	75.5	69.6
GAST [75]	83.9	<u>56.7</u>	76.4	55.0	73.4	72.2	69.5
GAI [53]	<b>85.8</b>	55.3	77.2	55.4	73.8	72.4	70.0
MLSP [36]	83.7	55.4	77.1	<u>55.6</u>	<u>78.2</u>	76.1	71.0
3DeNet [70]	84.5	<b>57.1</b>	78.8	<b>57.2</b>	<u>77.5</u>	<u>78.1</u>	<u>72.2</u>
ZS-CLIP [47]	46.1	17.0	52.0	17.0	52.0	46.1	38.4
PointCLIP [71]	50.8	20.9	50.1	20.9	50.1	50.8	40.6
PointCLIPv2 [74]	38.8	19.5	71.6	19.5	71.6	38.8	43.3
CLIPoint3D-T	74.4	9.5	86.0	24.1	50.5	59.8	50.7
CLIPoint3D-V	<u>84.6</u>	53.5	<b>91.6</b>	55.3	<b>87.9</b>	81.3	<b>75.7</b>
CLIPoint3D-B	81.5	51.9	90.3	46.6	85.2	<b>85.8</b>	73.6
Improvement	<b>-1.2</b>	<b>-3.6</b>	<b>+11.8</b>	<b>-1.9</b>	<b>+9.7</b>	<b>+7.7</b>	<b>+3.5</b>

#### 4.1. Comparisons to the Literature

Table 1 and 2 detail the comparative analysis of CLIPoint3D against leading conventional encoder-based and CLIP-based approaches. Suffixes ‘T’, ‘V’, and ‘B’ indicate LoRA fine-tuning on CLIP’s text, vision, and both encoders, respectively.

**Results on PointDA-10.** Table 1 shows that zero-shot CLIP variants (PointCLIP, PointCLIPv2, ZS-CLIP) underperform encoder-based methods, particularly on the challenging *ScanNet* domain. While encoder-based models capture geometric cues more effectively, they still lag behind our CLIPoint3D. Across all source-target pairs, CLIPoint3D achieves the best average accuracy, surpassing prior approaches by at least **3.5%**. Although it shows minor drops in certain cases (e.g., ScanNet adaptation), it yields substantial gains in synthetic domains (*ModelNet*, *ShapeNet*), ranking second for ModelNet $\rightarrow$ ShapeNet.

**Results on GraspNetPC-10.** Table 2 highlights that encoder-based methods exhibit unstable synthetic-to-real performance, especially under *Kinect* and *Realsense* sensors. In contrast, CLIPoint3D achieves consistent improvements with an average margin of **16.4%** across all adaptation directions. It maintains strong generalization under both synthetic-to-real and real-to-real shifts. Zero-shot CLIP baselines remain weak in transferability, underscoring their limited 3D adaptability. Overall, CLIPoint3D delivers the most balanced and robust results, effectively bridging vision-language pretraining with 3D adaptation.

#### 5. Ablation Studies

**(i) Impact of PEFT methods.** Table 3 compares PEFT adaptation strategies such as LayerNorm tuning [28], BitFit [67], and LoRA [12, 24, 56, 68] within CLIPoint3D.

Table 2. **Domain adaptation performance on the GraspNetPC-10 benchmark.** Syn.: Synthetic domain, Kin.: Kinect domain, RS.: Realsense domain;  $\rightarrow$  indicates the adaptation direction.

Methods	Syn. $\rightarrow$ Kin.	Syn. $\rightarrow$ RS.	Kin. $\rightarrow$ RS.	RS. $\rightarrow$ Kin.	Avg
DANN [14]	78.6	70.3	46.1	67.9	65.7
PointDAN [45]	77.0	72.5	65.9	82.3	74.4
RS [51]	67.3	58.6	55.7	69.6	62.8
DefRec + PCM [2]	80.7	70.5	65.1	77.7	73.5
GAST [75]	69.8	61.3	58.7	70.6	65.1
GAI [53]	<u>81.2</u>	<u>73.1</u>	<u>66.4</u>	<u>82.6</u>	<u>75.8</u>
ZS-CLIP [47]	20.0	14.8	14.8	20.0	17.4
PointCLIP [71]	30.7	24.3	24.3	30.7	27.5
PointCLIPv2 [74]	30.3	22.8	22.8	30.3	26.6
CLIPoint3D-T	87.6	71.6	74.2	82.3	78.9
CLIPoint3D-V	95.0	85.0	<b>88.4</b>	94.3	90.7
CLIPoint3D-B	<b>96.5</b>	<b>89.3</b>	86.8	<b>96.2</b>	<b>92.2</b>
Improvement	<b>+15.3</b>	<b>+16.2</b>	<b>+22.0</b>	<b>+13.6</b>	<b>+16.4</b>

Table 3. **Ablation study of PEFT methods.** Here, ‘PT’ refers to our proposed knowledge-driven prompt tuning strategy. The results reported are the average performances on GraspNetPC-10.

Method	PEFT			PT	PEFT + PT		
	Text	Vision	Both	-	Text	Vision	Both
LoRA [24]	80.3	89.2	90.5		78.9	<u>90.7</u>	<b>92.2</b>
LayerNorm [28]	75.4	<b>84.0</b>	76.6	73.7	75.0	<u>79.5</u>	78.8
BitFit [67]	80.1	<u>87.8</u>	81.1		79.7	<b>88.5</b>	81.5

Table 4. **Ablation of different loss components.** The results reported are the average performance for benchmarks.

$\mathcal{L}_{ce}$	$\mathcal{L}_{ortho}$	$\mathcal{L}_{proto}$	$\mathcal{L}_{OT}$	$\mathcal{L}_{conf}$	PointDA-10	GraspNetPC-10
✓	✗	✗	✗	✗	49.8	64.3
✓	✓	✗	✗	✗	58.6	74.9
✓	✓	✓	✗	✗	64.5	80.3
✓	✓	✗	✓	✗	70.4	85.0
✓	✓	✗	✗	✓	71.3	81.9
✓	✓	✓	✓	✗	71.0	85.8
✓	✓	✗	✓	✓	73.9	86.3
✓	✓	✓	✗	✓	72.3	84.3
✓	✓	✓	✓	✓	<b>75.7</b>	<b>92.2</b>

Among the standalone methods, LoRA achieves the highest accuracy (90.5%), especially when jointly applied to both encoders, while BitFit and LayerNorm tuning offer limited gains. This shows that low-rank adaptation captures domain-specific cues more effectively than simple bias or normalization tuning. Combining LoRA with our proposed prompting method improves results (92.2%), confirming their complementarity in refining task-specific subspaces.

**(ii) Sensitivity to loss functions.** Table 4 reports the contribution of each loss term. The baseline with only  $\mathcal{L}_{ce}$ , as well as combinedly with  $\mathcal{L}_{ortho}$  and  $\mathcal{L}_{conf}$  showcase the lack of domain alignment and yield lower accuracy. Adding  $\mathcal{L}_{proto}$  improves semantic consistency, while  $\mathcal{L}_{OT}$  substantially reduces domain discrepancy. Optimizing all terms jointly achieves peak accuracy, 75.7% (PointDA-10) and 92.2% (GraspNetPC-10), demonstrating their roles.

**(iii) Ablation on prompting strategies.** Table 5 compares different prompting configurations. Using only textual prompts  $\mathbf{P}_t(\mathbf{q})$  or visual prompts  $\mathbf{P}_v(\mathbf{q})$  yields moderate

Table 5. **Analysis of our prompting strategy in PointDA-10 benchmark.** Explanations of the notations below are given in Section 3. M: ModelNet, S: ShapeNet, S\*: ScanNet.

Strategy	M→S	M→S*	S→M	S→S*	S*→M	S*→S	Avg
$P_t(\mathbf{q})$ only	80.1	45.6	84.4	44.3	81.5	72.3	68.0
$P_v(\mathbf{q})$ only	82.1	48.9	85.7	48.1	82.1	71.7	69.8
$P_t(\mathbf{q}) + P_v(\mathbf{q})$	<b>85.4</b>	50.8	90.8	48.4	87.5	71.3	72.4
$P_t(\mathbf{q}) + P_v(\mathbf{I}_{3D}, \mathbf{q})$	83.2	49.5	91.2	48.9	83.9	71.1	71.3
$P_t(\mathbf{T}^{\text{lim}}, \mathbf{q}) + P_v(\mathbf{q})$	81.4	52.3	91.2	49.2	84.5	<b>89.2</b>	74.6
$P_t(\mathbf{T}^{\text{lim}}, \mathbf{q}) + P_v(\mathbf{I}_{3D}, \mathbf{q})$	84.6	<b>53.5</b>	<b>91.6</b>	<b>55.3</b>	<b>87.9</b>	81.3	<b>75.7</b>

gains, with  $P_v$  performing slightly better due to geometric cues. Naive multimodal concatenation (MaPLe [27]) fails to exploit cross-modal complementarity effectively, but achieves better performance than unimodal prompting. In contrast, our LLM-guided textual prompts  $P_t(\mathbf{T}^{\text{lim}}, \mathbf{q})$  and 3D-conditioned visual prompts  $P_v(\mathbf{I}_{3D}, \mathbf{q})$  jointly achieve the highest accuracy (75.7%), confirming that semantic grounding and geometric awareness act synergistically to enable robust multimodal adaptation.

(iv) **Effects of number of shots.** Figure 3a shows performance under varying the supervision level in  $\mathcal{D}_s$ . Accuracy rises sharply from as the training set size in  $\mathcal{D}_s$  changes from 8 to 64, peaking at 75.7% and 92.2% on PointDA-10 and GraspNetPC-10, respectively, after which gains majorly saturate despite increasing the training data.

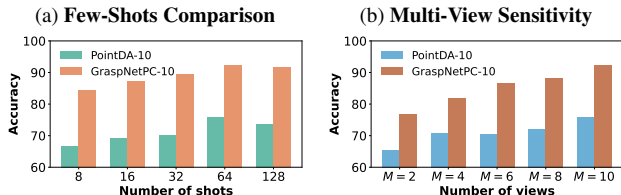


Figure 3. (a) Effect of the **number of labeled samples** in  $\mathcal{D}_s$  during training. (b) **Effect of projected views.** Accuracy variation with projection count  $M$ .

(v) **Influence of projected views.** As shown in Figure 3b, increasing the number of 2D projections  $M$  enhances performance by enriching multi-view cues. However, we achieve the maximum accuracy at  $M=10$ , where additional views are found to add redundancy with minimal gain.

(vi) **Effect of view selection.** Table 6 analyzes different view aggregation strategies. Averaging logits performs best, while weighted average or max-similarity driven selection slightly degrades results. Random selection causes a large drop, confirming the value of informed sampling. Our entropy-guided approach yields the top accuracy, prioritizing dominated views for stable multi-view representation.

(vii) **Computational complexity.** Table 7 compares model efficiency. While DANN and DefRec+PCM are lightweight but less accurate, large models like GAST (160M+ params) offer no advantage. CLIPPoint3D achieves the best trade-off, having only 9-11M trainable parameters with SOTA perfor-

Table 6. **Ablation of view selection strategies on GraspNetPC-10.** ‘Avg.’, ‘W. avg.’, and ‘Max Sim’ denote uniform averaging, weighted averaging, and maximum-similarity-driven logit selection. ‘Random’ selects a random single view, while ‘Entropy-guided’ is our proposed uncertainty-based selection scheme.

Method	Avg.	W. Avg	Random	Max Sim.	Entropy-guided
CLIPPoint3D-T	<b>82.5</b>	77.7	51.4	<u>80.1</u>	78.9
CLIPPoint3D-V	<b>91.5</b>	86.5	71.5	86.3	<u>90.7</u>
CLIPPoint3D-B	<u>92.0</u>	91.1	70.9	85.4	<b>92.2</b>

Table 7. **Trade-off between computational complexity and model performances.** Trainable parameters and accuracy are reported in millions (M) and %, respectively.

Methods	DANN	PointDAN	DAE-Global	DefRec+PCM	GAST
Train params. (M)	<b>2.50</b>	11.26	12.60	<b>2.50</b>	161.09
PointDA-10 (%)	56.8	56.3	63.1	69.6	69.5
GraspNetPC-10 (%)	65.7	74.4	-	73.5	65.1
Methods	GAI	MLSP	Ours-T	Ours-V	Ours-B
Train params. (M)	22.02	28.0	<u>9.24</u>	<u>9.83</u>	<u>11.00</u>
PointDA-10 (%)	70.0	<u>71.0</u>	50.7	<b>75.7</b>	73.6
GraspNetPC-10 (%)	<u>75.8</u>	-	78.9	90.7	<b>92.2</b>

mance on both benchmarks.

(viii) **Qualitative results.** Figure 4 visualizes source (synthetic) and target (Kinect) embeddings via t-SNE [39]. After adaptation, features form compact, overlapping clusters, indicating better alignment. Fréchet Distance [23] drops from 0.19 to 0.0009 and MMD [37] from 1.08 to 0.12, confirming improved cross-domain consistency.

In Supplementary, we provide (i) details of datasets, (ii) pseudocode algorithm, (iii) analysis of the LoRA rank, (iv) conventional plug-in UDA methods [14, 32, 38] in CLIP, (v) ablation of  $\alpha$  hyperparameter, (vi) length of  $\mathbf{q}$ , (vii) impact of CLIP backbones and (viii) effect of various LLMs [1, 18, 42, 66].

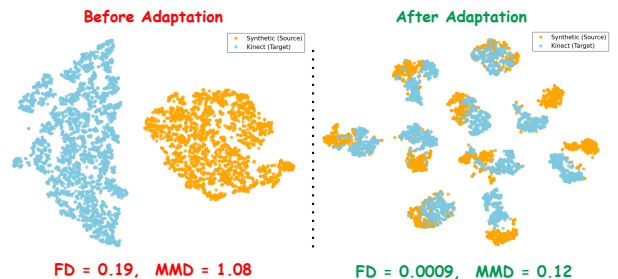


Figure 4. **t-SNE visualization** of CLIPPoint3D’s performance. Alignment between synthetic and real domains post-adaptation. FD and MMD quantify domain gap reduction.

## 6. Conclusions

In this work, we present CLIPPoint3D, a framework for few-shot unsupervised 3D point cloud domain adaptation built on CLIP. By integrating knowledge-driven prompt tuning,

parameter-efficient fine-tuning, and entropy-guided view sampling, CLIPPoint3D adapts vision-language models to 3D without retraining large encoders. Its optimal transport and uncertainty-aware prototype losses ensure robust domain alignment and class discriminability. Extensive results on PointDA-10 and GraspNetPC-10 show consistent gains over CLIP-based and encoder-based baselines. In future work, we plan to develop a progressive self-refinement pipeline where uncertainty-weighted prototypes iteratively guide pseudo-label re-estimation and view selection.

**Acknowledgements.** This work is supported in part by the European Commission’s Horizon 2020 Framework Programme through the Marie Skłodowska-Curie Action ANT (GA no. 101169439).

## References

- [1] Marah Abdin, Jyoti Aneja, Harkirat Behl, Sébastien Bubeck, Ronen Eldan, Suriya Gunasekar, Michael Harrison, Russell J Hewett, Mojan Javaheripi, Piero Kauffmann, et al. Phi-4 technical report. *arXiv preprint arXiv:2412.08905*, 2024. [2](#), [8](#), [12](#), [16](#)
- [2] Idan Achituve, Haggai Maron, and Gal Chechik. Self-supervised learning for domain adaptation on point clouds. In *Proceedings of the IEEE/CVF winter conference on applications of computer vision*, pages 123–133, 2021. [2](#), [7](#)
- [3] Fan Bai, Alan Ritter, and Wei Xu. Pre-train or annotate? domain adaptation with a constrained budget. *Proceedings of the 2021 Conference on Empirical Methods in Natural Language Processing*, 2021. [1](#)
- [4] Shai Ben-David, John Blitzer, Koby Crammer, and Fernando Pereira. Analysis of representations for domain adaptation. *Advances in neural information processing systems*, 19, 2006. [6](#)
- [5] Fabio Bracci, Martin Drauschke, Stefan Kühne, and Z-C Márton. Challenges in fusion of heterogeneous point clouds. *The International Archives of the Photogrammetry, Remote Sensing and Spatial Information Sciences*, 42:155–162, 2018. [1](#)
- [6] Angel X Chang, Thomas Funkhouser, Leonidas Guibas, Pat Hanrahan, Qixing Huang, Zimo Li, Silvio Savarese, Manolis Savva, Shuran Song, Hao Su, et al. Shapenet: An information-rich 3d model repository. *arXiv preprint arXiv:1512.03012*, 2015. [6](#), [12](#), [13](#)
- [7] Ali Cheraghian, Zeeshan Hayder, Sameera Ramasinghe, Shafin Rahman, Javad Jafaryahya, Lars Petersson, and Mehrtash Harandi. Canonical shape projection is all you need for 3d few-shot class incremental learning. In *European Conference on Computer Vision*, pages 36–53. Springer, 2024. [2](#), [3](#)
- [8] Angela Dai, Angel X Chang, Manolis Savva, Maciej Halber, Thomas Funkhouser, and Matthias Nießner. Scannet: Richly-annotated 3d reconstructions of indoor scenes. In *Proceedings of the IEEE conference on computer vision and pattern recognition*, pages 5828–5839, 2017. [6](#), [12](#), [13](#)
- [9] Jiuqian Dai, Zhenyan Ji, Zechang Xiong, Guiping Zhu, Hui Liu, Shen Yin, and Jose Enrique Armendariz-Inigo. Mvf-pointclip: Training-free multi-view fusion pointclip for zero-shot 3d classification. *Neurocomputing*, 653:131188, 2025. [2](#)
- [10] Zhekai Du, Xinyao Li, Fengling Li, Ke Lu, Lei Zhu, and Jingjing Li. Domain-agnostic mutual prompting for unsupervised domain adaptation. In *Proceedings of the IEEE/CVF Conference on Computer Vision and Pattern Recognition*, pages 23375–23384, 2024. [3](#)
- [11] Hao-Shu Fang, Chenxi Wang, Minghao Gou, and Cewu Lu. Graspnet-1billion: A large-scale benchmark for general object grasping. In *Proceedings of the IEEE/CVF conference on computer vision and pattern recognition*, pages 11444–11453, 2020. [6](#), [12](#), [13](#)
- [12] Matteo Farina, Massimiliano Mancini, Giovanni Iacca, and Elisa Ricci. Rethinking few-shot adaptation of vision-language models in two stages. In *Proceedings of the Computer Vision and Pattern Recognition Conference*, pages 29989–29998, 2025. [7](#)
- [13] Yaroslav Ganin and Victor Lempitsky. Unsupervised domain adaptation by backpropagation. In *International conference on machine learning*, pages 1180–1189. PMLR, 2015. [1](#)
- [14] Yaroslav Ganin, Evgeniya Ustinova, Hana Ajakan, Pascal Germain, Hugo Larochelle, François Laviolette, Mario March, and Victor Lempitsky. Domain-adversarial training of neural networks. *Journal of machine learning research*, 17(59):1–35. [1](#), [2](#), [5](#), [7](#), [8](#), [12](#), [14](#), [15](#)
- [15] Peng Gao, Shijie Geng, Renrui Zhang, Teli Ma, Rongyao Fang, Yongfeng Zhang, Hongsheng Li, and Yu Qiao. Clip-adapter: Better vision-language models with feature adapters. *International Journal of Computer Vision*, 132(2): 581–595, 2024. [14](#)
- [16] Chunjiang Ge, Rui Huang, Mixue Xie, Zihang Lai, Shiji Song, Shuang Li, and Gao Huang. Domain adaptation via prompt learning. *IEEE Transactions on Neural Networks and Learning Systems*, 2023. [3](#)
- [17] Ankit Goyal, Hei Law, Bowei Liu, Alejandro Newell, and Jia Deng. Revisiting point cloud shape classification with a simple and effective baseline. In *International conference on machine learning*, pages 3809–3820. PMLR, 2021. [4](#), [12](#)
- [18] Aaron Grattafiori, Abhimanyu Dubey, Abhinav Jauhri, Abhinav Pandey, Abhishek Kadian, Ahmad Al-Dahle, Aiesha Letman, Akhil Mathur, Alan Schelten, Alex Vaughan, et al. The llama 3 herd of models. *arXiv preprint arXiv:2407.21783*, 2024. [2](#), [8](#), [12](#), [16](#)
- [19] Kensho Hara, Hirokatsu Kataoka, and Yutaka Satoh. Can spatiotemporal 3d cnns retrace the history of 2d cnns and imagenet? In *Proceedings of the IEEE conference on Computer Vision and Pattern Recognition*, pages 6546–6555, 2018. [1](#)
- [20] Kaveh Hassani and Mike Haley. Unsupervised multi-task feature learning on point clouds. In *Proceedings of the IEEE/CVF international conference on computer vision*, pages 8160–8171, 2019. [7](#)
- [21] Weinan He, Yixin Zhang, and Zilei Wang. Progressive distribution bridging: Unsupervised adaptation for large-scale pre-trained models via adaptive auxiliary data. In *Proceed-*

- ings of the *IEEE/CVF International Conference on Computer Vision*, pages 3280–3292, 2025. 3
- [22] Deepti Hegde, Jeya Maria Jose Valanarasu, and Vishal Patel. Clip goes 3d: Leveraging prompt tuning for language grounded 3d recognition. In *Proceedings of the IEEE/CVF International Conference on Computer Vision*, pages 2028–2038, 2023. 2, 3
- [23] Martin Heusel, Hubert Ramsauer, Thomas Unterthiner, Bernhard Nessler, and Sepp Hochreiter. Gans trained by a two time-scale update rule converge to a local nash equilibrium. *Advances in neural information processing systems*, 30, 2017. 8
- [24] Edward J Hu, Yelong Shen, Phillip Wallis, Zeyuan Allen-Zhu, Yuanzhi Li, Shean Wang, Lu Wang, Weizhu Chen, et al. Lora: Low-rank adaptation of large language models. *ICLR*, 1(2):3, 2022. 4, 6, 7
- [25] Tianyu Huang, Bowen Dong, Yunhan Yang, Xiaoshui Huang, Rynson WH Lau, Wanli Ouyang, and Wangmeng Zuo. Clip2point: Transfer clip to point cloud classification with image-depth pre-training. In *Proceedings of the IEEE/CVF International Conference on Computer Vision*, pages 22157–22167, 2023. 2
- [26] Menglin Jia, Luming Tang, Bor-Chun Chen, Claire Cardie, Serge Belongie, Bharath Hariharan, and Ser-Nam Lim. Visual prompt tuning. In *European conference on computer vision*, pages 709–727. Springer, 2022. 4
- [27] Muhammad Uzair Khattak, Hanoona Rasheed, Muhammad Maaz, Salman Khan, and Fahad Shahbaz Khan. Maple: Multi-modal prompt learning. In *Proceedings of the IEEE/CVF conference on computer vision and pattern recognition*, pages 19113–19122, 2023. 4, 8
- [28] Konwoo Kim, Michael Laskin, Igor Mordatch, and Deepak Pathak. How to adapt your large-scale vision-and-language model. 2021. 7
- [29] Okan Kopuklu, Neslihan Kose, Ahmet Gunduz, and Gerhard Rigoll. Resource efficient 3d convolutional neural networks. In *Proceedings of the IEEE/CVF international conference on computer vision workshops*, pages 0–0, 2019. 1
- [30] Zhengfeng Lai, Noranart Vesdapunt, Ning Zhou, Jun Wu, Cong Phuoc Huynh, Xuelu Li, Kah Kuen Fu, and Chen-Nee Chuah. Padclip: Pseudo-labeling with adaptive debiasing in clip for unsupervised domain adaptation. In *Proceedings of the IEEE/CVF International Conference on Computer Vision*, pages 16155–16165, 2023. 3
- [31] Brian Lester, Rami Al-Rfou, and Noah Constant. The power of scale for parameter-efficient prompt tuning. *Proceedings of the 2021 Conference on Empirical Methods in Natural Language Processing*, 2021. 4
- [32] Shuang Li, Mixue Xie, Fangrui Lv, Chi Harold Liu, Jian Liang, Chen Qin, and Wei Li. Semantic concentration for domain adaptation. In *Proceedings of the IEEE/CVF international conference on computer vision*, pages 9102–9111, 2021. 1, 8, 12, 14, 15
- [33] Xinyao Li, Yuke Li, Zhekai Du, Fengling Li, Ke Lu, and Jingjing Li. Split to merge: Unifying separated modalities for unsupervised domain adaptation. In *Proceedings of the IEEE/CVF Conference on Computer Vision and Pattern Recognition*, pages 23364–23374, 2024. 3
- [34] Xiang Lisa Li and Percy Liang. Prefix-tuning: Optimizing continuous prompts for generation. *Proceedings of the 59th Annual Meeting of the Association for Computational Linguistics and the 11th International Joint Conference on Natural Language Processing (Volume 1: Long Papers)*, 2021. 4
- [35] Vladislav Lialin, Vijeta Deshpande, and Anna Rumshisky. Scaling down to scale up: A guide to parameter-efficient fine-tuning. arxiv 2023. *arXiv preprint arXiv:2303.15647*, 6, 2023. 2
- [36] Hanxue Liang, Hehe Fan, Zhiwen Fan, Yi Wang, Tianlong Chen, Yu Cheng, and Zhangyang Wang. Point cloud domain adaptation via masked local 3d structure prediction. In *European conference on computer vision*, pages 156–172. Springer, 2022. 1, 2, 7
- [37] Mingsheng Long, Yue Cao, Jianmin Wang, and Michael Jordan. Learning transferable features with deep adaptation networks. In *International conference on machine learning*, pages 97–105. PMLR, 2015. 1, 5, 8
- [38] Mingsheng Long, Zhangjie Cao, Jianmin Wang, and Michael I Jordan. Conditional adversarial domain adaptation. *Advances in neural information processing systems*, 31, 2018. 1, 8, 12, 14, 15
- [39] Laurens van der Maaten and Geoffrey Hinton. Visualizing data using t-sne. *Journal of machine learning research*, 9 (Nov):2579–2605, 2008. 8
- [40] Sachit Menon and Carl Vondrick. Visual classification via description from large language models. In *International Conference on Learning Representations*, 2023. 13
- [41] Munish Monga, Sachin Kumar Giroh, Ankit Jha, Mainak Singha, Biplab Banerjee, and Jocelyn Chanussot. Cosmo: Clip talks on open-set multi-target domain adaptation. *arXiv preprint arXiv:2409.00397*, 2024. 3
- [42] OpenAI. Introducing gpt-5. <https://openai.com/index/introducing-gpt-5/>, 2025. August 7, 2025. 2, 4, 6, 8, 12, 13, 16
- [43] Johannes Otepka, Sajid Ghuffar, Christoph Waldhauser, Ronald Hochreiter, and Norbert Pfeifer. Georeferenced point clouds: A survey of features and point cloud management. *ISPRS International Journal of Geo-Information*, 2 (4):1038–1065, 2013. 1
- [44] Charles R Qi, Hao Su, Kaichun Mo, and Leonidas J Guibas. Pointnet: Deep learning on point sets for 3d classification and segmentation. In *Proceedings of the IEEE conference on computer vision and pattern recognition*, pages 652–660, 2017. 1, 4, 6
- [45] Can Qin, Haoxuan You, Lichen Wang, C-C Jay Kuo, and Yun Fu. Pointdan: A multi-scale 3d domain adaption network for point cloud representation. *Advances in Neural Information Processing Systems*, 32, 2019. 1, 2, 6, 7, 13
- [46] Alec Radford, Karthik Narasimhan, Tim Salimans, Ilya Sutskever, et al. Improving language understanding by generative pre-training. <https://www.mikecaptain.com/resources/pdf/GPT-1.pdf>, 2018. 2
- [47] Alec Radford, Jong Wook Kim, Chris Hallacy, Aditya Ramesh, Gabriel Goh, Sandhini Agarwal, Girish Sastry,

- Amanda Askeell, Pamela Mishkin, Jack Clark, et al. Learning transferable visual models from natural language supervision. In *International conference on machine learning*, pages 8748–8763. PmLR, 2021. [2](#), [7](#), [15](#)
- [48] Taki Hasan Rafi, Ratul Mahjabin, Emon Ghosh, Young-Woong Ko, and Jeong-Gun Lee. Domain generalization for semantic segmentation: a survey. *Artificial Intelligence Review*, 57(9):247, 2024. [1](#)
- [49] Ievgen Redko, Amaury Habrard, and Marc Sebban. Theoretical analysis of domain adaptation with optimal transport. In *Joint European Conference on Machine Learning and Knowledge Discovery in Databases*, pages 737–753. Springer, 2017. [6](#)
- [50] Herbert Robbins and Sutton Monro. A stochastic approximation method. *The annals of mathematical statistics*, pages 400–407, 1951. [6](#)
- [51] Jonathan Sauder and Bjarne Sievers. Self-supervised deep learning on point clouds by reconstructing space. *Advances in neural information processing systems*, 32, 2019. [2](#), [7](#)
- [52] Sitian Shen, Zilin Zhu, Linqian Fan, Harry Zhang, and Xinxiao Wu. Diffclip: Leveraging stable diffusion for language grounded 3d classification. In *Proceedings of the IEEE/CVF Winter Conference on Applications of Computer Vision*, pages 3596–3605, 2024. [2](#)
- [53] Yuefan Shen, Yanchao Yang, Mi Yan, He Wang, Youyi Zheng, and Leonidas J Guibas. Domain adaptation on point clouds via geometry-aware implicit. In *Proceedings of the IEEE/CVF conference on computer vision and pattern recognition*, pages 7223–7232, 2022. [2](#), [6](#), [7](#), [13](#)
- [54] Manli Shu, Weili Nie, De-An Huang, Zhiding Yu, Tom Goldstein, Anima Anandkumar, and Chaowei Xiao. Test-time prompt tuning for zero-shot generalization in vision-language models. *Advances in Neural Information Processing Systems*, 35:14274–14289, 2022. [2](#)
- [55] Mainak Singha, Harsh Pal, Ankit Jha, and Biplab Banerjee. Ad-clip: Adapting domains in prompt space using clip. In *Proceedings of the IEEE/CVF International Conference on Computer Vision*, pages 4355–4364, 2023. [3](#)
- [56] Mainak Singha, Subhankar Roy, Sarthak Mehrotra, Ankit Jha, Moloud Abdar, Biplab Banerjee, and Elisa Ricci. Fed-mvp: Federated multimodal visual prompt tuning for vision-language models. In *Proceedings of the IEEE/CVF International Conference on Computer Vision*, pages 17869–17878, 2025. [7](#), [13](#)
- [57] Hang Su, Subhansu Maji, Evangelos Kalogerakis, and Erik Learned-Miller. Multi-view convolutional neural networks for 3d shape recognition. In *Proceedings of the IEEE international conference on computer vision*, pages 945–953, 2015. [4](#), [12](#)
- [58] Eric Tzeng, Judy Hoffman, Kate Saenko, and Trevor Darrell. Adversarial discriminative domain adaptation. In *Proceedings of the IEEE conference on computer vision and pattern recognition*, pages 7167–7176, 2017. [1](#)
- [59] Changshuo Wang, Xin Ning, Linjun Sun, Liping Zhang, Weijun Li, and Xiao Bai. Learning discriminative features by covering local geometric space for point cloud analysis. *IEEE Transactions on Geoscience and Remote Sensing*, 60: 1–15, 2022. [1](#)
- [60] Qi Wang, Jian Chen, Jianqiang Deng, and Xinfang Zhang. 3d-centernet: 3d object detection network for point clouds with center estimation priority. *Pattern Recognition*, 115: 107884, 2021. [1](#)
- [61] Ruibin Wang, Xianghua Ying, Bowei Xing, Xin Tong, Taiyan Chen, Jinfa Yang, and Yongjie Shi. Improving point cloud classification and segmentation via parametric veronese mapping. *Pattern Recognition*, 144:109784, 2023. [1](#)
- [62] Yue Wang, Yongbin Sun, Ziwei Liu, Sanjay E Sarma, Michael M Bronstein, and Justin M Solomon. Dynamic graph cnn for learning on point clouds. *ACM Transactions on Graphics (tog)*, 38(5):1–12, 2019. [1](#)
- [63] Zhirong Wu, Shuran Song, Aditya Khosla, Fisher Yu, Linguang Zhang, Xiaoou Tang, and Jianxiong Xiao. 3d shapenets: A deep representation for volumetric shapes. In *Proceedings of the IEEE conference on computer vision and pattern recognition*, pages 1912–1920, 2015. [6](#), [12](#), [13](#)
- [64] Tuo Xiang, Xuemiao Xu, Bangzhen Liu, Jinyi Li, Yong Li, and Shengfeng He. Seeing 3d through 2d lenses: 3d few-shot class-incremental learning via cross-modal geometric rectification. In *Proceedings of the IEEE/CVF International Conference on Computer Vision*, pages 6761–6771, 2025. [2](#), [3](#)
- [65] Wan Xu, Tianyu Huang, Tianyuan Qu, Guanglei Yang, Yiwen Guo, and Wangmeng Zuo. Filp-3d: Enhancing 3d few-shot class-incremental learning with pre-trained vision-language models. *Pattern Recognition*, 165:111558, 2025. [2](#), [3](#)
- [66] An Yang, Baosong Yang, Beichen Zhang, Binyuan Hui, Bo Zheng, Bowen Yu, Chengyuan Li, Dayiheng Liu, Fei Huang, Haoran Wei, et al. Qwen2. 5 technical report. *arXiv preprint arXiv:2412.15115*, 2024. [2](#), [8](#), [12](#), [16](#)
- [67] Elad Ben Zaken, Shauli Ravfogel, and Yoav Goldberg. Bit-fit: Simple parameter-efficient fine-tuning for transformer-based masked language-models. *Proceedings of the 60th Annual Meeting of the Association for Computational Linguistics (Volume 2: Short Papers)*, 2021. [7](#)
- [68] Maxime Zanella and Ismail Ben Ayed. Low-rank few-shot adaptation of vision-language models. In *Proceedings of the IEEE/CVF Conference on Computer Vision and Pattern Recognition*, pages 1593–1603, 2024. [7](#)
- [69] Yihan Zeng, Chenhan Jiang, Jiageng Mao, Jianhua Han, Chaoqiang Ye, Qingqiu Huang, Dit-Yan Yeung, Zhen Yang, Xiaodan Liang, and Hang Xu. Clip2: Contrastive language-image-point pretraining from real-world point cloud data. In *Proceedings of the IEEE/CVF conference on computer vision and pattern recognition*, pages 15244–15253, 2023. [3](#)
- [70] Huang Zhang, Xin Ning, Changshuo Wang, Enhao Ning, and Lusi Li. Deformation depth decoupling network for point cloud domain adaptation. *Neural Networks*, 180:106626, 2024. [2](#), [7](#)
- [71] Renrui Zhang, Ziyu Guo, Wei Zhang, Kunchang Li, Xupeng Miao, Bin Cui, Yu Qiao, Peng Gao, and Hongsheng Li. Pointclip: Point cloud understanding by clip. In *Proceedings of the IEEE/CVF conference on computer vision and pattern recognition*, pages 8552–8562, 2022. [2](#), [4](#), [5](#), [7](#), [15](#)
- [72] Zexuan Zhong, Dan Friedman, and Danqi Chen. Factual probing is [mask]: Learning vs. learning to recall. *Proceed-*

ings of the 2021 Conference of the North American Chapter of the Association for Computational Linguistics: Human Language Technologies, 2021. 4

- [73] Kaiyang Zhou, Jingkang Yang, Chen Change Loy, and Ziwei Liu. Learning to prompt for vision-language models. *International Journal of Computer Vision*, 130(9):2337–2348, 2022. 4
- [74] Xiangyang Zhu, Renrui Zhang, Bowei He, Ziyu Guo, Ziyao Zeng, Zipeng Qin, Shanghang Zhang, and Peng Gao. Point-clip v2: Prompting clip and gpt for powerful 3d open-world learning. In *Proceedings of the IEEE/CVF international conference on computer vision*, pages 2639–2650, 2023. 2, 7, 15
- [75] Longkun Zou, Hui Tang, Ke Chen, and Kui Jia. Geometry-aware self-training for unsupervised domain adaptation on object point clouds. In *Proceedings of the IEEE/CVF international conference on computer vision*, pages 6403–6412, 2021. 1, 2, 7

## Supplementary Contents

- Dataset descriptions:** In Table 8, we provide the total number of point cloud samples in the training and test splits of each domain of each datasets, though we do few-shot training in our proposed method.
- LLM attributes generation:** In Fig. 5, we show the pipeline of generation of high-level knowledge attributes using an LLM.
- Pseudo-code of the CLIPoint3D algorithm:** In Algorithm 1, we provide the detailed procedure of our proposed method through a pseudo-code.
- Analysis of the LoRA rank:** In Fig. 7 we showcase the effect of the rank of LoRA matrices in CLIPoint3D on both datasets.
- Conventional plug-in UDA methods in CLIP baselines:** In Table 9 we provide an analysis of training our CLIP-based zero-shot baselines using traditional UDA methods e.g. DANN [14], CDAN [38] and SCDA [32].
- Effect of  $\alpha$  hyperparameter:** In Fig. 8, we showcase the importance of  $\alpha$  hyperparameter used in the total loss function of Eq. 13.
- Influence of the length of prompt  $q$ :** In Fig. 9, we show the effect of shared prompt length in CLIPoint3D.
- Impact of CLIP variants:** In Table 10 we analyze the effect of CLIP backbones i.e. ViT-B/16, ViT-B/32 and ViT-L/14 in our proposed CLIPoint3D method.
- Effect of various LLMs:** We also ablate how the attributes generated from different LLMs e.g. GPT-5 [42], Llama-3.2-3B [18], Qwen2.5-14B [66], Phi-4 [1] etc can effect the performances of our method.

## A. Dataset descriptions

The PointDA-10 benchmark collects object point clouds from ModelNet40 [63], ShapeNet [6], and ScanNet [8], covering ten shared object categories. ModelNet-10 (M)

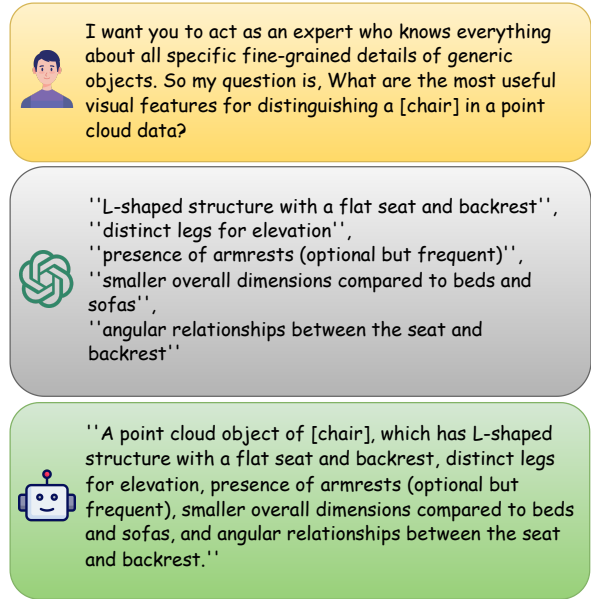


Figure 5. **LLM attributes generation.** To derive high-level 3D knowledge representations, we follow a three-stage pipeline. First (top box), we provide an instructional query prompt to a LLM (e.g. GPT-5 [42]). In response, the LLM produces detailed, geometry-aware visual descriptions (middle box). Finally (bottom box), we generate highly contextualized textual prompts (one caption per class) by combining a modality-specific prefix template with the LLM-generated attributes.

dataset contains 4,183 training and 856 testing samples obtained by following online perspective projection [17] unlike post rendering [57], i.e., simply projecting each point onto a series of pre-defined image planes to generate scatter depth maps. ShapeNet-10 (S) dataset includes 17,378 training and 2,492 testing point clouds, exhibiting greater structural diversity due to its larger number of object instances and wider geometric variation. ScanNet-10 (S\*) dataset consists of 6,110 training and 1,769 testing point clouds, containing sensor noise, occlusions, and missing surfaces inherent to reconstructed indoor scenes.

GraspNetPC-10 benchmark is constructed from GraspNet [11], a large-scale dataset designed for robotic grasping from raw depth scans and reconstructed CAD models. The point clouds are generated by re-projecting depth maps into 3D space and cropping objects using segmentation masks. Unlike PointDA-10, the point clouds in GraspNetPC-10 are not aligned. This benchmark includes three domains: Synthetic (Syn.), Kinect (Kin.), and Realsense (RS.), corresponding to CAD-rendered depth scans and raw sensor captures from two different depth cameras. The synthetic domain contains 12,000 training samples, while the

Table 8. Domain Generation dataset statistical details on class, training and test splits, prefix template.

Dataset	Domains	Common Classes	# Samples	# Training / Test
PointDA-10 [45]	ModelNet [63]	Bathtub, Bed, Bookshelf,	5039	4183 / 856
	ShapeNet [6]	Cabinet, Chair, Lamp,	19870	17378 / 2492
	ScanNet [8]	Monitor, Plant, Sofa, Table	7879	6110 / 1769
GraspNetPC-10 [11, 53]	Synthetic	Banana, Box, Can,	12,000	12,000 / -
	Kinect	Camel, Dish, Drill, Mouse,	13,533	10,973 / 2560
	Realsense	Pear, Scissors, Shampoo	13,258	10,698 / 2560

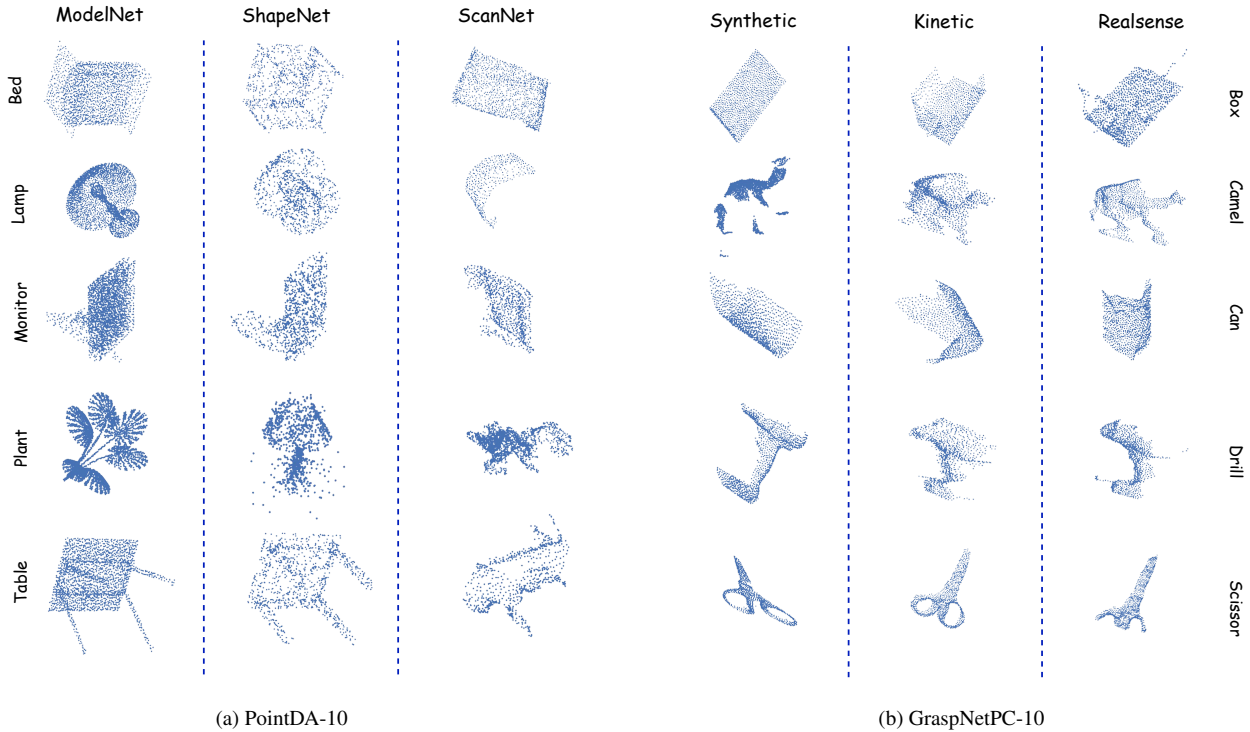


Figure 6. **Domain Visualization.** We show the diverse geometry variations across the domains of PointDA-10 and GraspNetPC-10 datasets.

Kinect and Realsense domains contain 10,973/2,560 and 10,698/2,560 training/testing samples, respectively. Real-world scans from two different depth cameras i.e. Kinect2 and Intel Realsense exhibit domain-specific artifacts, including varying noise patterns, geometric distortions, and missing regions.

In Figure 6, we show the diverse geometric variations of different point cloud class objects in synthetic (ModelNet, ShapeNet, Synthetic) and real-world (ScanNet, Kinect, Realsense) environments on both the PointDA-10 and GraspNetPC-10 benchmarks.

## B. LLM attributes generation

To generate descriptive attributes for each class, we leverage an LLM i.e. GPT-5 [42]. Each class label is passed through a structured instructional prompt, adapted and expanded from the template proposed in [40], as shown in Figure 5. Specifically, We follow a three-stage pipeline similar to [56] to construct the attributes integrating two complementary components: a modality-specific prefix template and the attribute set produced by the LLM. First, we design a prefix that is tailored to the imaging modality of interest i.e. `''A point cloud object of [class]''`. We then propose a way to enrich this prefix by appending the combination of the LLM-generated at-

tributes on a single sentence using connective phrases such as which is a/an'' or which has'', i.e. a single descriptive attribute for each class, which is different from others. This yields a semantically detailed and context-aware prompt that captures both modality information and discriminative visual characteristics. A complete example for the class ``chair'' is shown in the third row of Figure 5.

### C. Pseudo-code of CLIPoint3D

In Algorithm 1 we provide the detailed pseudo-codes of training and inference process of CLIPoint3D algorithm.

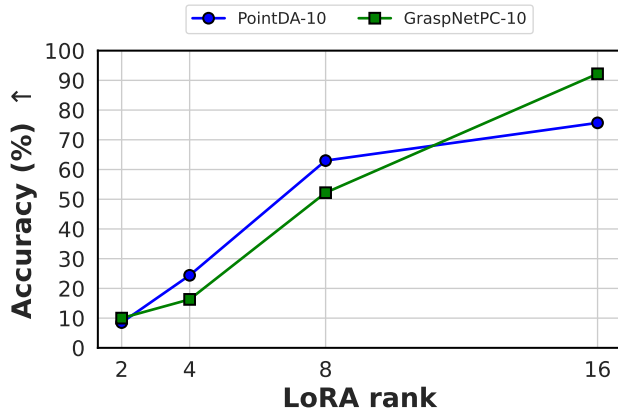


Figure 7. **Effect of varying LoRA rank.** We report the adaptation performances of CLIPoint3D on PointDA-10 and GraspNetPC-10 datasets.

### D. Analysis of the LoRA rank

To understand the influence of the low-rank decomposition on adaptation quality, we conduct an ablation study on LoRA ranks 2, 4, 8 & 16 using our CLIPoint3D framework across the PointDA-10 and GraspNetPC-10 benchmarks. As shown in Figure 7, increasing the LoRA rank consistently improves performance, but the rate of improvement differs markedly between the two datasets.

On PointDA-10, which contains relatively clean synthetic CAD models alongside noisier real scans, accuracy improves steadily from rank 2 to rank 16. The sharp gain from rank 4 to rank 8 indicates that a moderate rank is essential to capture the geometric variability and structural inconsistencies across domains. Beyond rank 8, the improvement becomes more modest, suggesting diminishing returns as representational capacity saturates. Whereas on GraspNetPC-10, whose features are more complex real-world sensor noise and greater intra-class variation, the benefit of increasing the LoRA rank is even more pronounced. Performance rises from rank 2 to rank 16, with a substan-

tial leap between rank 8 and rank 16. The results show that higher-rank LoRA modules in CLIPoint3D provide the expressive adaptability and generalizability on realistic depth distortions, object incompleteness, and viewpoint variability present in the point cloud domains.

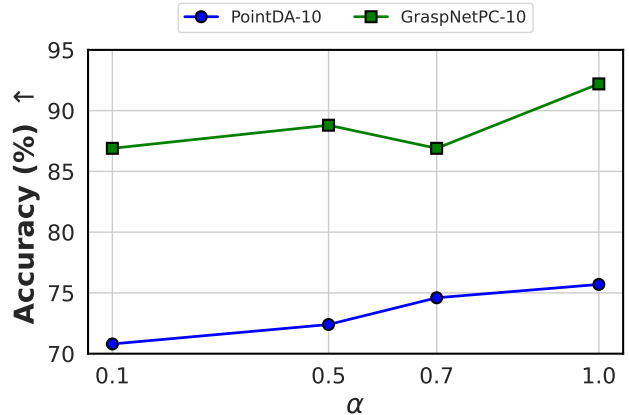


Figure 8. **Effect of varying  $\alpha$  hyperparameter.** We report the adaptation performances of CLIPoint3D on PointDA-10 and GraspNetPC-10 datasets.

### E. Conventional plug-in UDA methods in CLIP baselines

In Table 9, we evaluate the effect of integrating standard UDA techniques e.g. DANN [14], CDAN [38], and SCDA [32] into our CLIP-based baselines (Zs-CLIP, PointCLIP & PointCLIPv2) to train them for point-cloud UDA task. While these conventional UDA methods can bring modest improvements in certain cross-domain transfers, their gains are inconsistent and often fail to fully bridge the domain gap inherent in 3D point cloud data. To be noted, we have just added a learnable adapter on top of the frozen visual features of the vision encoder similar to [15], while keeping both the encoders entirely frozen. While the CLIP-based methods improve adaptation after pluggin on the UDA methods, but still underperform compared to CLIPoint3D variants. It highlights the limitations of applying traditional 2D-centric UDA strategies directly to CLIP-based 3D recognition. The results of Table 9 suggest that while conventional UDA provides some benefits, more specialized adaptation strategies are necessary to consistently leverage the cross-modal representations of CLIP and achieve robust performance across diverse 3D domains.

### F. Effect of $\alpha$ hyperparameter

We investigate the influence of the  $\alpha$  hyperparameter in the total loss function (Eq. 13 of main paper) in our proposed CLIPoint3D. As shown in Fig. 8, varying  $\alpha$  affects

Table 9. **Comparison of plug-in UDA methods in CLIP baselines with CLIPoint3D.** We report the adaptation performances on the PointDA-10 benchmark. M: ModelNet, S: ShapeNet, S\*: ScanNet;  $\rightarrow$  indicates the adaptation direction. Best results and second-best results are reported in bold and underlined, respectively.

Methods	M $\rightarrow$ S	M $\rightarrow$ S*	S $\rightarrow$ M	S $\rightarrow$ S*	S* $\rightarrow$ M	S* $\rightarrow$ S	Avg
ZS-CLIP [47]	46.1	17.0	52.0	17.0	52.0	46.1	38.4
CLIP [47] + DANN [14]	62.0	8.6	77.3	10.5	56.7	50.4	44.3
CLIP + CDAN [38]	60.9	7.0	76.5	11.0	56.7	50.0	43.7
CLIP + SCDA [32]	46.5	16.2	51.2	17.0	51.8	46.2	38.2
PointCLIP [71]	50.8	20.9	50.1	20.9	50.1	50.8	40.6
PointCLIP [71] + DANN	55.3	9.8	74.2	14.3	50.4	49.7	42.3
PointCLIP + CDAN	55.8	9.2	72.1	13.7	50.9	49.3	41.8
PointCLIP + SCDA	39.2	17.6	70.9	19.8	67.6	37.6	42.1
PointCLIPv2 [74]	38.8	19.5	71.6	19.5	71.6	38.8	43.3
PointCLIP [71] + DANN	46.2	12.2	80.4	13.6	79.5	40.6	45.4
PointCLIP + CDAN	44.6	12.8	75.7	12.9	76.8	41.7	44.1
PointCLIP + SCDA	45.9	12.0	74.8	12.5	77.2	40.2	43.8
<b>CLIPoint3D-T</b>	74.4	9.5	86.0	24.1	50.5	59.8	50.7
<b>CLIPoint3D-V</b>	<b>84.6</b>	<b>53.5</b>	<b>91.6</b>	<b>55.3</b>	<b>87.9</b>	<b>81.3</b>	<b>75.7</b>
<b>CLIPoint3D-B</b>	<u>81.5</u>	<u>51.9</u>	<u>90.3</u>	46.6	<u>85.2</u>	<b>85.8</b>	<u>73.6</u>

Table 10. **Effect of using various CLIP variants on CLIPoint3D.** We report the adaptation performances on the PointDA-10 benchmark.

Methods	ViT-B/16	ViT-B/32	ViT-L/14
ModelNet $\rightarrow$ ShapeNet	84.6	82.4	85.7
ModelNet $\rightarrow$ ScanNet	53.5	42.7	54.4
ShapeNet $\rightarrow$ ModelNet	91.6	88.3	92.1
ShapeNet $\rightarrow$ ScanNet	55.3	36.9	59.5
ScanNet $\rightarrow$ ModelNet	87.9	88.2	88.5
ScanNet $\rightarrow$ ShapeNet	81.3	73.7	82.3
Average	75.7	68.7	77.1

the trade-off between different components of the loss and consequently the adaptation performance. For PointDA-10, increasing  $\alpha$  leads to a steady improvement, indicating that a higher weight on the corresponding loss term better guides the model for cross-domain alignment. In contrast, GraspNetPC-10 exhibits a more varied trend, with performance peaking at intermediate and higher  $\alpha$  values, suggesting that overly small or excessively large weighting can underutilize certain loss components.

## G. Influence of the prompt length

We analyze the effect of the length of shared prompt  $q$  on CLIPoint3D. As shown in Fig. 9, varying  $q$  affects the UDA performances on both PointDA-10 and GraspNetPC-10 benchmarks. For PointDA-10, the performance remains relatively stable across different  $q$  values, indicating that CLIPoint3D is robust to moderate changes in prompt length. In contrast, GraspNetPC-10 exhibits slight fluctuations, with intermediate values of  $q$  yielding the best results.

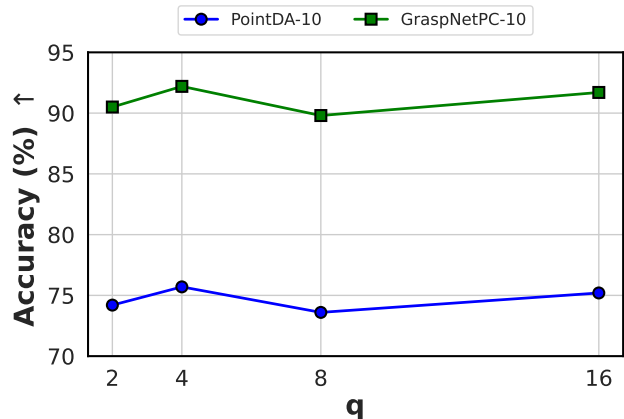


Figure 9. **Effect of varying length of  $q$ .** We report the adaptation performances of CLIPoint3D on PointDA-10 and GraspNetPC-10 datasets.

## H. Impact of CLIP variants

We investigate how different CLIP backbone architectures affect the performance of our CLIPoint3D method. Table 10 compares results using ViT-B/16, ViT-B/32, and ViT-L/14. Overall, larger frozen ViT backbones tend to provide stronger feature representations, leading to improved domain adaptation performance. Specifically, ViT-L/14 achieves the highest average accuracy, benefiting from its larger model capacity and fine-grained patch representation. ViT-B/16 offers a strong trade-off between efficiency and performance, outperforming ViT-B/32 in most cases despite similar model sizes. It indicates that the choice of backbone has a significant impact on the effectiveness of cross-domain alignment, while showcasing CLIP has the extreme

Table 11. **Effect of using different LLMs on CLIPoint3D for attributes generation.** We report the adaptation performances on the GraspNetPC-10 benchmark.

Methods	Llama-3.2-3B[18]	Qwen2.5-14B [66]	Phi-4[1]	GPT-5[42]
Synthetic→Kinect	95.5	95.0	95.8	96.5
Synthetic→Realsense	84.1	87.5	83.2	89.3
Kinect→Realsense	84.3	83.2	79.6	86.8
Realsense→Kinect	95.6	95.4	92.3	96.2
Average	89.9	90.3	87.7	<b>92.2</b>

potential of capturing better the nuances of 3D point cloud distributions.

## I. Effect of various LLMs

We examine the impact of using different LLMs to generate semantic attributes for our method CLIPoint3D. Table 11 summarizes the adaptation performance when attributes are derived from GPT-5 [42], Llama-3.2-3B [18], Qwen2.5-14B [66], and Phi-4 [1]. Across all adaptation scenarios, GPT-5 consistently produces the most informative attributes, leading to the highest average performance. While other LLMs such as Llama-3.2-3B and Qwen2.5-14B yield competitive results in certain domain pairs, their overall effectiveness is slightly lower and more variable. The results highlight that the quality and expressiveness of the generated attributes significantly influence cross-domain alignment, emphasizing the importance of selecting a capable LLM for robust 3D domain adaptation.

---

**Algorithm 1** CLIPoint3D algorithm

---

**Require:** Training data: source domain  $\mathcal{D}^{S_l} = \{(P_i^{S_l}, y_i^{S_l})\}_{i=1}^{N_{S_l}} = \{(x_{i,m}^{S_l}, y_i^{S_l})\}$  and target domain  $\mathcal{D}^{\mathcal{T}_u} = \{P_j^{\mathcal{T}_u}\}_{j=1}^{N_{\mathcal{T}_u}} = \{x_{j,m}^{\mathcal{T}_u}\}$ ,  $\mathcal{E}_t$ ,  $\mathcal{E}_v$  &  $\mathcal{E}_{3D}$ .

- 1: **procedure** TRAINING OBJECTIVE
  - 2:     Generate the attributes of set of classes,  $\mathcal{C} = \{c_k\}_{k=1}^K$ , by a LLM, and extract  $\mathbf{T}^{\text{llm}}$  using Eq.2.
  - 3:     Generate  $M$  2D projected depth maps for each 3D point cloud sample.
  - 4:     Initialize a random prompt vector of length  $l$  from a Gaussian distribution.
  - 5:     **if**  $n = 1$  **then** ▷ Given total  $\mathcal{N}$  epochs
  - 6:         **for**  $i \leftarrow 0$  **to**  $K$  **do** ▷ Given  $K$  iterations
  - 7:             Generate textual prompts  $\mathbf{P}_t(\mathbf{T}^{\text{llm}}, \mathbf{p})$  using Eq.3, and extract textual embeddings  $\mathbf{T}$  from  $\mathcal{E}_t$ .
  - 8:             Generate source and target visual prompts ( $\mathbf{P}_v^S$  &  $\mathbf{P}_v^{\mathcal{T}_u}$ ) separately using Eq.4.
  - 9:             Extract visual embeddings  $\mathbf{I}_{S_l}$  and  $\mathbf{I}_{\mathcal{T}_u}$  from  $\mathcal{E}_v^S$  &  $\mathcal{E}_v^{\mathcal{T}_u}$  respectively.
  - 10:             Do PEFT adaptation of text / vision / both encoder(s).
  - 11:             Select the views of minimum entropy using Eq.5 and calculate the final prediction probability of a point cloud sample using Eq.6.
  - 12:             Calculate  $\mathbf{L}_{ce}$ ,  $\mathbf{L}_{ortho}$ ,  $\mathbf{L}_{OT}$  &  $\mathbf{L}_{conf}$  using Eq.13.
  - 13:             Append the source batch probabilities  $p_{S_l}$  in a list.
  - 14:             **end for**
  - 15:             Save all  $p_{S_l}$  and calculate uncertainty-weighted source class prototypes using Eq.7.
  - 16:             **end if**
  - 17:             **for**  $n \leftarrow 2$  **to**  $\mathcal{N}$  **do**
  - 18:                 Repeat the procedure of steps 7-15.
  - 19:                 Calculate  $\mathbf{L}_{proto}$  using the source prototypes from the  $(n - 1)$ -th epoch and Eq.10.
  - 20:                 Calculate  $\mathbf{L}_{total}$  using Eq.13.
  - 21:             **end for**
  - 22:     **end procedure**
  - 23: **procedure** INFERENCE
  - 24:     Consider all test samples of target domain  $\mathcal{D}^{\mathcal{T}_u}$  in the source dataloader and calculate  $\text{top-1}$  accuracy by selecting the class of maximum  $p_{\mathcal{T}_u}$ .
  - 25: **end procedure**
-